Multistatic Detection for Passive Radar With Direct-Path Interference

XIN ZHANG
HONGBIN LI, Senior Member, IEEE
Stevens Institute of Technology, Hoboken, NJ, USA

BRAHAM HIMED, Fellow, IEEE
AFRL/RYMD, Dayton, OH, USA

This paper examines the target detection problem in a multistatic passive radar with one noncooperative illuminator of opportunity (IO) and multiple distributed receivers. Specifically, we consider how to address the direct-path interference (DPI), which refers to the direct transmission from the IO to a receiver, to enhance passive detection performance. The DPI is in general much stronger (by many tens to even over a hundred dB) than the target echo. It is standard for a passive radar to apply some kind of interference cancellation by using, e.g., an adaptive array, to reduce the DPI. However, due to practical limitations of such techniques and the significant difference in strength between the DPI and target signal, the residual DPI after cancellation is often at a nonnegligible level. Unlike most existing passive detectors which ignore such residual DPI, we consider explicitly its effect and develop two new detectors under the conditions when the noise level is known and, respectively, when it is unknown. Another distinction from existing solutions is that the proposed detectors exploit the correlation of the IO waveform for passive detection. The proposed detectors are developed within the generalized likelihood ratio test (GLRT) framework, which involves nonlinear estimation that is solved using the expectation-maximization algorithm. Numerical results are presented to illustrate the performance of the proposed methods and several well-known passive detectors.

Manuscript received October 21, 2015; revised June 11, 2016; released for publication November 9, 2016. Date of publication February 9, 2017; date of current version April 27, 2017.

DOI. No. 10.1109/TAES.2017.2667223

Refereeing of this contribution was handled by S. Watts.

This work was supported in part by a subcontract with Matrix Research, Inc., for research sponsored by the Air Force Research Laboratory, and in part by the National Science Foundation under Grant ECCS-1609393.

Authors' addresses: X. Zhang and H. Li are with the Department of Electrical and Computer Engineering, Stevens Institute of Technology, Hoboken, NJ 07030 USA, E-mail: (xzhang23@stevens.edu; Hongbin.Li@stevens.edu); B. Himed is with the AFRL/RYMD, Dayton, OH 45433 USA, E-mail: (braham.himed@us.af.mil).

I. INTRODUCTION

A passive radar system can detect and track targets of interest by utilizing noncooperative illuminators of opportunity (IOs), such as radio, television, and cellular signals [1]–[4]. Passive radar is attracting considerable interest recently due to several advantages compared with an active system. Specifically, because a passive radar does not transmit, it is naturally covert and offers high tolerance to electronic countermeasure. It does not require additional spectrum and has been widely considered as a unique sensing capability to cope with the radio spectrum congestion problem. In addition, a passive radar can readily employ a multistatic configuration by using several IOs and/or several receivers at different locations, which leads to spatial diversity and improved sensing capabilities [5].

Passive radar can be broadly classified into two categories, based on whether a reference channel (RC) is employed. In the first category, an RC is utilized at the receiver to collect the direct-path (transmitter-to-receiver) signal, while a separate surveillance channel (SC) is used to collect the target echo [1]–[4], [6]. A standard detector for such passive systems is based on the cross-correlation (CC) operation between the RC and SC, which mimics the matched filtering (MF) approach used in active radar. In particular, the reference signal obtained with the RC plays the role of the transmitted signal in the MF operation. In [7], several improved detectors were developed by taking into account the effect of the noise in the RC. The effect of noise is also examined in [8] in a passive multiinput multioutput (MIMO) radar setup. The second category avoids a dedicated RC that may be difficult to implement in some practical scenarios where a high-quality reference signal is not accessible. One idea is to employ multichannel observations (e.g., via multiple spatially distributed sensors) of the target echo and exploit the interchannel correlations for target estimation and detection [9]–[15]. Since the receivers collect target echoes due to the illumination of the same IO, a correlation exists among the multiple observations. Therefore, the target detection problem is equivalent to determining the presence or absence of a common but unknown signal in these independent noisy observations. For digital modulation based IOs, a reference signal can be obtained by demodulating the received signal, which allows the passive radar to bypass a dedicated RC (see [16] and references therein).

In this paper, we consider target detection for multistatic passive radar without RC. There are several notable solutions to this problem. The energy detector (ED) is a well-known method for detecting an unknown signal in white noise, which measures the received signal energy and compares it with the noise level that is assumed known [17], [18]. A generalized canonical correlation (GCC) detector was developed in [10] and [11], which uses the largest eigenvalue of the Gram matrix as its test variable. Like the ED, the GCC detector needs to know the noise level to properly set the test threshold. The magnitude-squared coherence (MSC) detector [19] does not need the noise

level; however, it is limited to the two-receiver case. An extended version of the MSC, known as the generalized coherence (GC) detector which can cope with any number of receivers, was introduced in [20] and [21]. The GC detector was rederived in [13] using a Bayesian framework. Another detector for passive radar without requiring the noise level was introduced in [14], which is referred to as the RLET detector as its test variable is the ratio of the largest eigenvalue to the trace of the Gram matrix.

A passive radar has to employ some kind of interference cancellation technique to cope with the direct-path interference (DPI), e.g., using an antenna array with a null formed in the direction of the IO, and/or a temporal filter that employs the reference signal in the RC to cancel the DPI [22]–[25]. A standard approach is to treat DPI cancellation and target detection as two separate processes [24]. The first step is primarily concerned with interference cancellation, whereas the second step is target detection, assuming the absence of any residual interference. However, some residual DPI may still exist after the initial cancellation. In particular, the direct-path signal is generally significantly stronger (by many tens to even over a hundred dB) compared with the target echo [26], [27]. Nonnegligible DPI in the SC may be caused by noise in the RC, limited array size, and/or mismatch between the null of the array beam pattern and the real IO direction. As a result, the DPI may still be at a nonnegligible power level compared with the target echo. To address this issue, we consider a joint interference cancellation and target detection problem, and propose solutions to explicitly take into account the residual DPI for weak target detection. This is one of the main contributions of this paper. Another contribution of this paper is that we aim to utilize the waveform correlation of the IO signal to solve the joint cancellation and detection problem. Here, the *correlation* refers to the *autocorrelation* of the IO waveform, that is, how adjacent samples of the waveform are statistically related to each other. Most existing methods treat the IO signal as either deterministic or stochastic with unknown and temporally uncorrelated samples. In practice, the IO waveform often exhibits some temporal correlation which can be exploited to improve the sensing performance.

We examine herein the target detection problem for a passive multistatic radar system without RC, where the receivers are contaminated by nonnegligible noise and DPI. We model the transmitted signal as a stochastic process, whose temporal correlation is exploited for detection. We present two solutions, based on the generalized likelihood ratio test (GLRT) framework, for this detection problem. The first detector assumes that the receiver noise level is known. In this case, the noise level has to be estimated in advance by some estimation procedure. However, such estimation may be subject to errors. Hence, we also consider a second case where the receiver noise level is unknown. For both cases, the maximum likelihood (ML) estimates of the unknown parameters, which are required by the GLRT, cannot be obtained in closed form. We resort to an expectation-maximization (EM) procedure [28] to find these estimates.

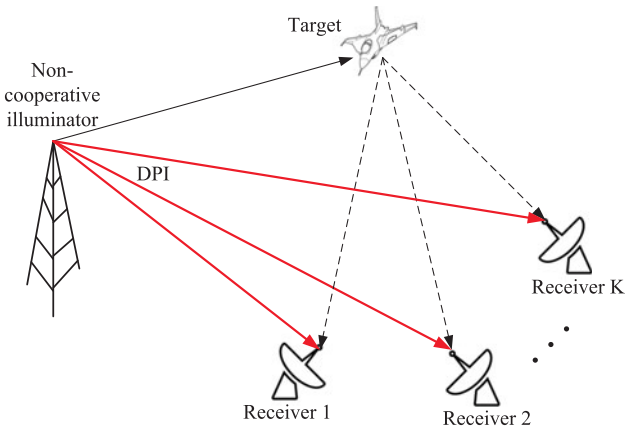

Fig. 1. Configuration of a multistatic passive radar system with the presence of DPI (solid red line).

Numerical results are provided to show the performance of the proposed detectors and compare with existing solutions.

The remainder of the paper is organized as follows. In Section II, we present the system model and formulate the problem of interest. In Section III, the proposed GLRT detectors are derived. Numerical results and discussions are included in Section IV, followed by conclusions in Section V.

Notation: Vectors (matrices) are denoted by boldface lower (upper) case letters, and all vectors are column vectors. Superscripts $(\cdot)^*$, $(\cdot)^T$, and $(\cdot)^H$ denote complex conjugate, transpose, and complex conjugate transpose, respectively. $\Re\{\cdot\}$ represents the real part of a complex quantity, $E\{\cdot\}$ denotes statistical expectation, and $\jmath$ stands for the imaginary unit. $\mathbf{0}_{p\times q}$ denotes a $p \times q$ matrix with all zero entries, $\mathbf{I}_N$ denotes an identity matrix of size N, $[\cdot]_{m,n}$ denotes the (m,n)th entry of a matrix, and $[\cdot]_m$ denotes the mth element of a vector. $\odot$ and $\otimes$ stand for the Hadamard and the Kronecker products, respectively. The notation $\mathcal{CN}$ denotes a circularly symmetric, complex Gaussian distribution. $\det\{\cdot\}$ represents the determinant of a matrix, $\|\cdot\|$ is the Frobenius norm, and $\mathrm{tr}\{\cdot\}$ denotes the trace of a matrix.

II. PROBLEM FORMULATION

Consider a multistatic passive radar, as depicted in Fig. 1, which contains one noncooperative illuminator of opportunity (IO) and K geographically distributed receivers for collecting the echoes from a target of interest due to the illumination of the IO. The signal collected by the kth receiver (channel), denoted by $y_k'(t)$, can be expressed as

$$y_k'(t) = \beta_k x(t-d_k) + \alpha_k' x(t-t_k) e^{\jmath 2\pi f_k t} + n_k'(t) \quad (1)$$

where $k = 1, 2, \ldots, K$, $x(t)$ is the unknown signal (baseband equivalent) transmitted by the IO, d_k is the propagation delay from the IO to the kth receiver, i.e., the propagation delay of the DPI, t_k is the propagation delay of the target, due to the transmission from the IO to the target and then from the target to the kth receiver, f_k is the target's Doppler frequency seen at the kth receiver, β_k is the scaling coefficient that includes the antenna attenuation and the channel

propagation effects from the IO to the kth receiver, α_k' is the scaling coefficient accounting for the target reflectivity, the antenna gain, and the channel propagation effects, and $n_k'(t)$ is the additive zero-mean white Gaussian noise on the kth channel with power (variance) η_k.

To simplify the system model, we observe that the direct-path delay d_k is generally known *a priori* and can be compensated for, since the location of the IO is usually known to each receiver. Let $y_k(t) = y_k'(t + d_k)$ denote the kth delay-compensated signal, and the delay-compensated noise $n_k(t)$ is similarly defined. This leads to

$$y_k(t) = \beta_k x(t) + \alpha_k x(t - \tau_k) e^{\jmath 2\pi f_k t} + n_k(t) \tag{2}$$

where τ_k is the kth bistatic delay given $\tau_k = t_k - d_k$ and $\alpha_k = \alpha_k' e^{\jmath 2\pi f_k d_k}$.

We assume that $x(t)$ has a duration of T s, e.g., due to the framed transmissions employed by the IO, in which case T represents the frame duration. The observation interval T_o is selected such that $T_o \geq T + \tau_{\max}$, where $\tau_{\max}$ denotes the maximum bistatic delay that can be tolerated by the system. We sample each channel using a sampling frequency $f_s \geq 2(B + f_{D_{\max}})$, where B denotes the bandwidth of the communication signal $x(t)$ and $f_{D_{\max}}$ is the maximum Doppler frequency of the target that is designed detectable by the system. Suppose M samples are collected for each channel over the observation window T_o, i.e., $T_o = MT_s$, where $T_s = 1/f_s$ denotes the sampling interval. Let $\bar{\mathbf{y}}_k = [y_k(0), y_k(T_s), \ldots, y_k((M-1)T_s)]^T$, $\bar{\mathbf{x}}_d(\tau_k) = [x(0 - \tau_k), x(T_s - \tau_k), \ldots, x((M-1)T_s - \tau_k)]^T$, and $\bar{\mathbf{x}}$ and $\bar{\mathbf{n}}_k$ be similarly defined $M \times 1$ vectors formed from samples of $x(t)$ and $n_k(t)$, respectively. The discrete model becomes

$$\bar{\mathbf{y}}_k = \beta_k \bar{\mathbf{x}} + \alpha_k \bar{\mathbf{x}}_d(\tau_k) \odot \bar{\mathbf{a}}(f_k) + \bar{\mathbf{n}}_k,\ k = 1, 2, \ldots, K \tag{3}$$

where $\odot$ stands for the Hadamard product and

$$\bar{\mathbf{a}}(f_k) = [1, e^{\jmath 2\pi f_k T_s}, \ldots, e^{\jmath 2\pi f_k (M-1) T_s}]^T. \tag{4}$$

In this paper, the signal waveform is modeled as a correlated stochastic process. Specifically, $\bar{\mathbf{x}}$ is zero-mean Gaussian distributed with covariance matrix $\mathbf{R}_x$. This stochastic model is justified for IOs involving sophisticated modulation techniques, such as the orthogonal frequency division multiplexing used in many wireless systems, which use multiple random information streams to form a composite transmitted signal [29]. According to the central limit theorem, this waveform can be modeled as a complex Gaussian process. In addition, the channel noise $\bar{\mathbf{n}}_k$ is a zero-mean white Gaussian noise with covariance matrix $\eta_k \mathbf{I}_M$, where the noise variance η_k may be unknown.

Let $\mathbf{y}_k = \mathbf{T}\bar{\mathbf{y}}_k$ denote the M-point discrete Fourier transform (DFT) of $\bar{\mathbf{y}}_k$, where the DFT matrix $\mathbf{T}$ has entries $[\mathbf{T}]_{p,q} = e^{-\jmath 2\pi (p-1)\Delta f (q-1) T_s}/\sqrt{M}$, $p, q = 1, 2, \ldots, M$, with the frequency domain sample spacing $\Delta f = \frac{f_s}{M} = \frac{1}{T_s M}$, and $\mathbf{x}$, $\mathbf{n}_k$, $\mathbf{a}(f_k)$ are $M \times 1$ vectors similarly obtained by the DFT. In particular,

$$\mathbf{a}(f_k) = [A_k(0), A_k(\Delta f), \ldots, A_k((M-1)\Delta f)]^T \tag{5}$$

where

$$A_k(m\Delta f) = \begin{cases} \sqrt{M}, & \text{if } m = \frac{f_k}{\Delta f} \\ \dfrac{1 - e^{\jmath 2\pi \left(\frac{f_k}{\Delta f} - m\right)}}{\sqrt{M}\left[1 - e^{\jmath \frac{2\pi}{M}\left(\frac{f_k}{\Delta f} - m\right)}\right]}, & \text{otherwise} \end{cases} \tag{6}$$

for $m = 0, 1, \ldots, M-1$. Applying basic DFT properties [30], the signal in the frequency domain for the kth channel can be written as

$$\mathbf{y}_k = \beta_k \mathbf{x} + \alpha_k \mathbf{A}(f_k)\mathbf{W}(\tau_k)\mathbf{x} + \mathbf{n}_k \tag{7}$$

where $\mathbf{A}(f_k)$ is the circulant matrix formed from the vector $\mathbf{a}(f_k)$, and $\mathbf{W}(\tau_k)$ is a diagonal matrix with diagonal entries $[\mathbf{W}(\tau_k)]_{p,p} = e^{-\jmath 2\pi \Delta f (p-1)\tau_k}$ for $p = 1, 2, \ldots, M$. Since the discrete sequence $\{A_k(m\Delta f)\}$ is periodic with period M, we have $A_k((M-m)\Delta f) = A_k((-m)\Delta f)$. Hence, we can write $\mathbf{A}(f_k)$ as

$$[\mathbf{A}(f_k)]_{p,q} = \frac{1}{\sqrt{M}} A_k((p-q)\Delta f),\ p, q = 1, 2, \ldots, M. \tag{8}$$

Clearly, $\mathbf{x}$ and $\mathbf{n}_k$ are Gaussian random vectors with zero mean and covariance matrices $\mathbf{C}_x = \mathbf{T}\mathbf{R}_x\mathbf{T}^H$ and $\eta_k \mathbf{I}_M$, respectively. Herein, we assume that the covariance matrix $\mathbf{R}_x$, i.e., the covariance matrix of the IO waveform $\bar{\mathbf{x}}$ in the time domain, is known *a priori*, and so is $\mathbf{C}_x$. Practically, the covariance matrix can be estimated from an auxiliary observation that contains the IO signal and possible channel noise (e.g., with an antenna steered toward the IO direction). This is how $\mathbf{R}_x$ was estimated in our simulation results shown in Section IV.

As a standard practice in radar signal detection [31], we consider testing for the presence of a target within a hypothesized delay-Doppler cell. Specifically, the target is assumed to be within an uncertainty region that is divided into multiple delay-Doppler cells and the detection is performed on each cell in a sequential fashion. For each cell under test, τ_k and f_k are known and can be compensated for. Therefore, after the data are delay- and Doppler-compensated, the detection problem can be described by the following composite binary hypothesis test [7]–[10], [14]:

$$\begin{aligned} &\mathcal{H}_1 : \mathbf{y}_k = \beta_k \mathbf{x} + \alpha_k \mathcal{D}_k \mathbf{x} + \mathbf{n}_k \\ &\mathcal{H}_0 : \mathbf{y}_k = \beta_k \mathbf{x} + \mathbf{n}_k, \\ &\qquad k = 1, 2, \ldots, K \end{aligned} \tag{9}$$

where the amplitude parameters β_k and α_k are unknown and need to be estimated, and the unitary matrix $\mathcal{D}_k$ is the kth delay-Doppler operator with respect to the hypothesized cell,

$$\mathcal{D}_k = \mathbf{A}(f_k)\mathbf{W}(\tau_k). \tag{10}$$

III. PROPOSED DETECTORS

In this section, we develop two GLRT detectors for the passive multistatic detection problem (9). The first is for the case of known receiver noise level, and the second is derived with unknown noise level.

A. GLRT With Known Noise Power

Let the observations from K receivers be vectorized as $\mathbf{y} = [\mathbf{y}_1^T, \mathbf{y}_2^T, \ldots, \mathbf{y}_K^T]^T$. The unknown parameters are $\boldsymbol{\beta} = [\beta_1, \beta_2, \ldots, \beta_K]^T$ and $\boldsymbol{\alpha} = [\alpha_1, \alpha_2, \ldots, \alpha_K]^T$. We can rewrite the detection problem (9) as

$$\begin{aligned} \mathcal{H}_1 &: \mathbf{y} \sim \mathcal{CN}(\mathbf{0}_{MK\times 1}, \mathbf{C}_y(\boldsymbol{\alpha}, \boldsymbol{\beta})) \\ \mathcal{H}_0 &: \mathbf{y} \sim \mathcal{CN}(\mathbf{0}_{MK\times 1}, \mathbf{C}_y(\boldsymbol{\alpha} = \mathbf{0}, \boldsymbol{\beta})) \end{aligned} \tag{11}$$

where the covariance matrix is given by

$$\begin{aligned} \mathbf{C}_y(\boldsymbol{\alpha}, \boldsymbol{\beta}) = (\boldsymbol{\beta}\boldsymbol{\beta}^H) \otimes \mathbf{C}_x + \mathbf{C}_n + [(\boldsymbol{\beta}\boldsymbol{\alpha}^H) \otimes \mathbf{C}_x]\mathbf{D}^H \\ + \mathbf{D}[(\boldsymbol{\alpha}\boldsymbol{\beta}^H) \otimes \mathbf{C}_x] + \mathbf{D}[(\boldsymbol{\alpha}\boldsymbol{\alpha}^H) \otimes \mathbf{C}_x]\mathbf{D}^H \end{aligned} \tag{12}$$

with the Kronecker product operation $\otimes$, block diagonal matrices $\mathbf{C}_n = \text{diag}\{\boldsymbol{\eta}\} \otimes \mathbf{I}_M$, by denoting $\boldsymbol{\eta} = [\eta_1, \eta_2, \ldots, \eta_K]^T$, and $\mathbf{D} = \text{diag}\{\mathcal{D}_1, \mathcal{D}_2 \ldots, \mathcal{D}_K\}$. Then, the GLRT may be given by

$$\frac{\max_{\{\boldsymbol{\alpha},\boldsymbol{\beta}\}} p_1(\mathbf{y}|\boldsymbol{\alpha}, \boldsymbol{\beta})}{\max_{\{\boldsymbol{\beta}\}} p_0(\mathbf{y}|\boldsymbol{\beta})} \underset{\mathcal{H}_0}{\overset{\mathcal{H}_1}{\gtrless}} \gamma \tag{13}$$

where $p_1(\mathbf{y}|\boldsymbol{\alpha}, \boldsymbol{\beta})$ and $p_0(\mathbf{y}|\boldsymbol{\beta})$ denote the likelihood functions under $\mathcal{H}_1$ and $\mathcal{H}_0$, respectively. The two ML estimation problems in (13) do not have closed-form solutions. A brute force search over the multidimensional parameter space is computationally difficult. In the following, we resort to the EM algorithm to solve the ML estimation problems, and the estimates are used in the GLRT detector.

To apply the EM algorithm under each hypothesis, the first step is to specify the "complete" data $\mathbf{z}$, which includes the observed data $\mathbf{y}$ (regarded as the "incomplete" data) [28]. In our case, the "complete" data are specified as

$$\mathbf{z} = \left[\mathbf{x}^T,\ \mathbf{y}^T\right]^T. \tag{14}$$

After determining the "complete" data, the EM algorithm starts with an initial guess of the unknown parameters, $\hat{\boldsymbol{\theta}}^{(0)}$ ($\boldsymbol{\theta} = \{\boldsymbol{\alpha}, \boldsymbol{\beta}\}$ under $\mathcal{H}_1$; $\boldsymbol{\theta} = \boldsymbol{\beta}$ under $\mathcal{H}_0$). Given the latest update for the parameter estimation after l iterations, $\hat{\boldsymbol{\theta}}^{(l)}$, the $(l+1)$th iteration cycle consists of an expectation step (E-step) followed by a maximization step (M-step):

E-step:

$$Q\left(\boldsymbol{\theta}; \hat{\boldsymbol{\theta}}^{(l)}\right) = E_{\mathbf{x}|\mathbf{y},\hat{\boldsymbol{\theta}}^{(l)}}\left\{\log p(\mathbf{z}|\boldsymbol{\theta})\right\}. \tag{15}$$

M-step:

$$\hat{\boldsymbol{\theta}}^{(l+1)} = \arg\max_{\boldsymbol{\theta}} Q\left(\boldsymbol{\theta}; \hat{\boldsymbol{\theta}}^{(l)}\right). \tag{16}$$

The E-step is intended to find the expectation of the log-likelihood function (LLF) of the "complete" data $\mathbf{z}$, which is taken with respect to the signal waveform $\mathbf{x}$ and conditioned on observations $\mathbf{y}$ given $\hat{\boldsymbol{\theta}}^{(l)}$. The M-step is intended to maximize the expectation with respect to the unknown parameters. This iteration cycle is repeated until the algorithm converges, e.g., when the following inequality holds for some small tolerance ϵ:

$$\left\|\hat{\boldsymbol{\theta}}^{(l+1)} - \hat{\boldsymbol{\theta}}^{(l)}\right\| < \epsilon. \tag{17}$$

It is shown in Appendix A that, for the $(l+1)$th iteration cycle, the M-step (16) under $\mathcal{H}_1$ is equivalent to

$$\hat{\boldsymbol{\theta}}^{(l+1)} = \arg\min_{\boldsymbol{\theta}} Q_1\left(\boldsymbol{\theta}; \hat{\boldsymbol{\theta}}^{(l)}\right) \tag{18}$$

where

$$\begin{aligned} Q_1\left(\boldsymbol{\theta}; \hat{\boldsymbol{\theta}}^{(l)}\right) = \sum_{k=1}^{K} \frac{1}{\eta_k}\Big[\left(|\beta_k|^2 + |\alpha_k|^2\right) c_1^{(l)} \\ + 2\Re\left\{\alpha_k \beta_k^* c_{2,k}^{(l)} - \beta_k c_{3,k}^{(l)} - \alpha_k c_{4,k}^{(l)}\right\}\Big] \end{aligned} \tag{19}$$

with $c_1^{(l)}$, $c_{2,k}^{(l)}$, $c_{3,k}^{(l)}$, and $c_{4,k}^{(l)}$ as defined in (54)–(57), which are functions of $\hat{\mathbf{x}}^{(l)}$ and $\mathbf{C}_{xx|y}^{(l)}$, namely, the minimum mean square error (MMSE) estimates of $\mathbf{x}$ and its covariance matrix, respectively, based on the lth parameter estimate $\hat{\boldsymbol{\theta}}^{(l)}$. The expressions of $\hat{\mathbf{x}}^{(l)}$ and $\mathbf{C}_{xx|y}^{(l)}$ are given by (51) and (52), respectively.

It can be seen that the cost function (19) is a quadratic function with respect to α_k and β_k for $k = 1, 2, \ldots, K$, and thus permits closed-form solutions. Specifically, taking the partial derivatives of the cost function with respect to the conjugates of α_k and β_k and setting them equal to zero, we have

$$\begin{cases} \alpha_k c_1^{(l)} + \beta_k \left(c_{2,k}^{(l)}\right)^* - \left(c_{4,k}^{(l)}\right)^* = 0 \\ \beta_k c_1^{(l)} + \alpha_k c_{2,k}^{(l)} - \left(c_{3,k}^{(l)}\right)^* = 0 \end{cases}. \tag{20}$$

Jointly solving the two expressions of (20) yields

$$\hat{\alpha}_k^{(l+1)} = \frac{\left(c_1^{(l)} c_{4,k}^{(l)} - c_{2,k}^{(l)} c_{3,k}^{(l)}\right)^*}{\left(c_1^{(l)}\right)^2 - \left|c_{2,k}^{(l)}\right|^2}, \tag{21}$$

$$\hat{\beta}_k^{(l+1)} = \frac{c_1^{(l)} \left(c_{3,k}^{(l)}\right)^* - c_{2,k}^{(l)} \left(c_{4,k}^{(l)}\right)^*}{\left(c_1^{(l)}\right)^2 - \left|c_{2,k}^{(l)}\right|^2}. \tag{22}$$

Under $\mathcal{H}_0$, the received data are free of target echoes, and the unknown parameters are $\boldsymbol{\theta} = \boldsymbol{\beta}$. The ML estimates under this hypothesis can be derived by repeating the steps under $\mathcal{H}_1$ with $\{\alpha_k\}$ set to zero, which are given by

$$\hat{\beta}_k^{(l+1)} = \frac{\left(c_{3,k}^{(l)}\right)^*}{c_1^{(l)}}. \tag{23}$$

After the EM iteration converges, let $\{\hat{\boldsymbol{\alpha}}_1, \hat{\boldsymbol{\beta}}_1\}$ and $\hat{\boldsymbol{\beta}}_0$ be the final estimates of the unknown parameters under $\mathcal{H}_1$ and

Algorithm 1: GLRT with Known Noise Power.

Input: K-channel observations $\mathbf{y}$, a specific delay-Doppler cell, initial guess of the parameters $\{\hat{\boldsymbol{\alpha}}^{(0)}, \hat{\boldsymbol{\beta}}^{(0)}\}$, and convergence tolerance ϵ.
Output: $\mathcal{L}_1$ as computed by (24).
Estimation of $\boldsymbol{\theta} = \{\boldsymbol{\alpha}, \boldsymbol{\beta}\}$ under $\mathcal{H}_1$:
for $l = 0, 1, 2, \ldots$ **do**
1) Compute the MMSE estimates $\hat{\mathbf{x}}^{(l)}$ and $\mathbf{C}_{xx|y}^{(l)}$ using (49)–(52).
2) Update the estimates of α_k and β_k using (21) and (22), respectively, for $k = 1, 2, \ldots, K$.
3) Check the stopping condition (17).
end for
Estimation of $\boldsymbol{\theta} = \boldsymbol{\beta}$ under $\mathcal{H}_0$:
for $l = 0, 1, 2, \ldots$ **do**
1) Compute the MMSE estimates $\hat{\mathbf{x}}^{(l)}$ and $\mathbf{C}_{xx|y}^{(l)}$ using (49)–(52) with $\hat{\boldsymbol{\alpha}}^{(l)} = \mathbf{0}$.
2) Update the estimates of β_k using (23) for $k = 1, 2, \ldots, K$.
3) Check the stopping condition (17).
end for
return

$\mathcal{H}_0$, respectively. The GLRT detector can be written as

$$\begin{aligned}\mathcal{L}_1 =& \log p_1(\mathbf{y}|\hat{\boldsymbol{\alpha}}_1, \hat{\boldsymbol{\beta}}_1) - \log p_0(\mathbf{y}|\hat{\boldsymbol{\beta}}_0) \\ =& \mathbf{y}^H \left[\mathbf{C}_y^{-1}(\mathbf{0}, \hat{\boldsymbol{\beta}}_0) - \mathbf{C}_y^{-1}(\hat{\boldsymbol{\alpha}}_1, \hat{\boldsymbol{\beta}}_1)\right]\mathbf{y} \\ &+ \ln \frac{\det\left\{\mathbf{C}_y(\mathbf{0}, \hat{\boldsymbol{\beta}}_0)\right\}}{\det\left\{\mathbf{C}_y(\hat{\boldsymbol{\alpha}}_1, \hat{\boldsymbol{\beta}}_1)\right\}} \underset{\mathcal{H}_0}{\overset{\mathcal{H}_1}{\gtrless}} \xi \end{aligned} \tag{24}$$

where $\xi = \ln\gamma$. The proposed detector is summarized in Algorithm 1.

B. GLRT With Unknown Noise Power

In this section, we consider the case of unknown receiver noise level, which can be different from one receiver to another, i.e., $\eta_1 \neq \eta_2 \neq \cdots \neq \eta_K$. Borrowing the notations from Section III-A, the detection problem is expressed as

$$\begin{aligned}\mathcal{H}_1 &: \mathbf{y} \sim \mathcal{CN}(\mathbf{0}_{MK\times 1}, \mathbf{C}_y(\boldsymbol{\alpha}, \boldsymbol{\beta}, \boldsymbol{\eta})) \\ \mathcal{H}_0 &: \mathbf{y} \sim \mathcal{CN}(\mathbf{0}_{MK\times 1}, \mathbf{C}_y(\boldsymbol{\alpha} = \mathbf{0}, \boldsymbol{\beta}, \boldsymbol{\eta}))\end{aligned} \tag{25}$$

where

$$\begin{aligned}\mathbf{C}_y(\boldsymbol{\alpha}, \boldsymbol{\beta}, \boldsymbol{\eta}) =& (\boldsymbol{\beta}\boldsymbol{\beta}^H) \otimes \mathbf{C}_x + \mathbf{C}_n(\boldsymbol{\eta}) + [(\boldsymbol{\beta}\boldsymbol{\alpha}^H) \otimes \mathbf{C}_x]\mathbf{D}^H \\ &+ \mathbf{D}[(\boldsymbol{\alpha}\boldsymbol{\beta}^H) \otimes \mathbf{C}_x] + \mathbf{D}[(\boldsymbol{\alpha}\boldsymbol{\alpha}^H) \otimes \mathbf{C}_x]\mathbf{D}^H\end{aligned} \tag{26}$$

with $\mathbf{C}_n(\boldsymbol{\eta}) = \text{diag}\{\boldsymbol{\eta}\} \otimes \mathbf{I}_M$. Consequently, the GLRT is given by

$$\frac{\max_{\{\boldsymbol{\alpha},\boldsymbol{\beta},\boldsymbol{\eta}\}} p_1(\mathbf{y}|\boldsymbol{\alpha}, \boldsymbol{\beta}, \boldsymbol{\eta})}{\max_{\{\boldsymbol{\beta},\boldsymbol{\eta}\}} p_0(\mathbf{y}|\boldsymbol{\beta}, \boldsymbol{\eta})} \underset{\mathcal{H}_0}{\overset{\mathcal{H}_1}{\gtrless}} \zeta \tag{27}$$

where $p_1(\mathbf{y}|\boldsymbol{\alpha}, \boldsymbol{\beta}, \boldsymbol{\eta})$ and $p_0(\mathbf{y}|\boldsymbol{\beta}, \boldsymbol{\eta})$ denote the likelihood functions under $\mathcal{H}_1$ and $\mathcal{H}_0$, respectively. Again, we use the EM algorithm to develop the GLRT detector in the following.

As shown in Appendix B, the $(l+1)$th M-step under $\mathcal{H}_1$, where the unknown parameters $\boldsymbol{\theta} = \{\boldsymbol{\alpha}, \boldsymbol{\beta}, \boldsymbol{\eta}\}$, is equivalent to

$$\hat{\boldsymbol{\theta}}^{(l+1)} = \arg\min_{\boldsymbol{\theta}} Q_2\big(\boldsymbol{\theta}; \hat{\boldsymbol{\theta}}^{(l)}\big) \tag{28}$$

where

$$Q_2\big(\boldsymbol{\theta}; \hat{\boldsymbol{\theta}}^{(l)}\big) = \sum_{k=1}^{K}\left(M\ln\eta_k + \frac{\hat{\Delta}^{(l)}(\alpha_k, \beta_k)}{\eta_k}\right) \tag{29}$$

and

$$\begin{aligned}\hat{\Delta}^{(l)}(\alpha_k, \beta_k) =& \ \|\mathbf{y}_k\|^2 + \left(|\beta_k|^2 + |\alpha_k|^2\right) c_1^{(l)} \\ &+ 2\Re\left\{\alpha_k\beta_k^* c_{2,k}^{(l)} - \beta_k c_{3,k}^{(l)} - \alpha_k c_{4,k}^{(l)}\right\}.\end{aligned} \tag{30}$$

The coefficients $c_1^{(l)}$, $c_{2,k}^{(l)}$, $c_{3,k}^{(l)}$, and $c_{4,k}^{(l)}$ have the same expressions as (54)–(57). Although the MMSE estimates $\hat{\mathbf{x}}^{(l)}$ and $\mathbf{C}_{xx|y}^{(l)}$ are still computed using (51) and (52), respectively, it should be noted that (50) must be replaced by (66) in this case. Since the noise variance $\eta_k > 0$, the $(l+1)$th updates of α_k and β_k can be obtained as

$$\left\{\hat{\alpha}_k^{(l+1)}, \hat{\beta}_k^{(l+1)}\right\} = \arg\min_{\{\alpha_k,\beta_k\}} \hat{\Delta}^{(l)}(\alpha_k, \beta_k). \tag{31}$$

Using the same optimization method for α_k and β_k, as in Section III-A, we find that $\hat{\alpha}_k^{(l+1)}$ and $\hat{\beta}_k^{(l+1)}$ have the same expressions as (21) and (22), respectively. Then, the kth noise variance is updated by

$$\hat{\eta}_k^{(l+1)} = \frac{\hat{\Delta}^{(l)}\left(\hat{\alpha}_k^{(l+1)}, \hat{\beta}_k^{(l+1)}\right)}{M}. \tag{32}$$

Under $\mathcal{H}_0$, the unknown parameters are $\boldsymbol{\theta} = \{\boldsymbol{\beta}, \boldsymbol{\eta}\}$. Similar to the null hypothesis in Section III-A, the ML estimates under $\mathcal{H}_0$ in this case can be derived by repeating the steps under $\mathcal{H}_1$ with $\boldsymbol{\alpha}$ set to zero. Consequently, $\hat{\beta}_k^{(l+1)}$ is given by (23), and

$$\hat{\eta}_k^{(l+1)} = \frac{\hat{\Delta}^{(l)}\left(0, \hat{\beta}_k^{(l+1)}\right)}{M}. \tag{33}$$

Let $\{\hat{\boldsymbol{\alpha}}_1, \hat{\boldsymbol{\beta}}_1, \hat{\boldsymbol{\eta}}_1\}$ and $\{\hat{\boldsymbol{\beta}}_0, \hat{\boldsymbol{\eta}}_0\}$ be the final EM estimates of the unknown parameters under $\mathcal{H}_1$ and $\mathcal{H}_0$, respectively. The second proposed GLRT detector can be written as

$$\begin{aligned}\mathcal{L}_2 =& \log p_1(\mathbf{y}|\hat{\boldsymbol{\alpha}}_1, \hat{\boldsymbol{\beta}}_1, \hat{\boldsymbol{\eta}}_1) - \log p_0(\mathbf{y}|\hat{\boldsymbol{\beta}}_0, \hat{\boldsymbol{\eta}}_0) \\ =& \mathbf{y}^H \left[\mathbf{C}_y^{-1}(\mathbf{0}, \hat{\boldsymbol{\beta}}_0, \hat{\boldsymbol{\eta}}_0) - \mathbf{C}_y^{-1}(\hat{\boldsymbol{\alpha}}_1, \hat{\boldsymbol{\beta}}_1, \hat{\boldsymbol{\eta}}_1)\right]\mathbf{y} \\ &+ \ln \frac{\det\left\{\mathbf{C}_y(\mathbf{0}, \hat{\boldsymbol{\beta}}_0, \hat{\boldsymbol{\eta}}_0)\right\}}{\det\left\{\mathbf{C}_y(\hat{\boldsymbol{\alpha}}_1, \hat{\boldsymbol{\beta}}_1, \hat{\boldsymbol{\eta}}_1)\right\}} \underset{\mathcal{H}_0}{\overset{\mathcal{H}_1}{\gtrless}} \kappa\end{aligned} \tag{34}$$

where $\kappa = \ln\zeta$. The proposed detector is summarized in Algorithm 2.

Algorithm 2: GLRT with Unknown Noise Power.

Input: K-channel observations $\mathbf{y}$, a specific delay-Doppler cell, initial guess of the parameters $\{\hat{\boldsymbol{\alpha}}^{(0)}, \hat{\boldsymbol{\beta}}^{(0)}, \hat{\boldsymbol{\eta}}^{(0)}\}$, and convergence tolerance ϵ.
Output: $\mathcal{L}_2$ as computed by (34).
Estimation of $\boldsymbol{\theta} = \{\boldsymbol{\alpha}, \boldsymbol{\beta}, \boldsymbol{\eta}\}$ under $\mathcal{H}_1$:
for $l = 0, 1, 2, \ldots$ **do**
1) Compute the MMSE estimates $\hat{\mathbf{x}}^{(l)}$ and $\mathbf{C}_{xx|y}^{(l)}$ using (49), (66), (51), and (52).
2) Update the estimates of α_k, β_k, and η_k using (21), (22), and (32), respectively, for $k = 1, 2, \ldots, K$.
3) Check the stopping condition (17).
end for
Estimation of $\boldsymbol{\theta} = \{\boldsymbol{\beta}, \boldsymbol{\eta}\}$ under $\mathcal{H}_0$:
for $l = 0, 1, 2, \ldots$ **do**
1) Compute the MMSE estimates $\hat{\mathbf{x}}^{(l)}$ and $\mathbf{C}_{xx|y}^{(l)}$ using (49), (66), (51), and (52) with $\hat{\boldsymbol{\alpha}}^{(l)} = \mathbf{0}$.
2) Update the estimates of β_k and η_k using (23) and (33), respectively, for $k = 1, 2, \ldots, K$.
3) Check the stopping condition (17).
end for
return

IV. NUMERICAL SIMULATIONS

In this section, numerical simulations are conducted to illustrate the performance of the proposed detectors. For comparison purposes, the ED [17], [18] and GCC [10], [11] detectors, which require knowledge of the noise level to set the test threshold, as well as the GC [20], [21] and RLET [14] detectors, which do not need the noise level, are included in the study. Their test statistics are expressed as

$$\mathcal{L}_{\text{ED}} = \sum_{k=1}^{K} \|\mathbf{y}_k\|^2 \underset{\mathcal{H}_0}{\overset{\mathcal{H}_1}{\gtrless}} \gamma_{\text{ED}} \tag{35}$$

$$\mathcal{L}_{\text{GCC}} = \lambda_1\left(\mathbf{Y}^H\mathbf{Y}\right) \underset{\mathcal{H}_0}{\overset{\mathcal{H}_1}{\gtrless}} \gamma_{\text{GCC}} \tag{36}$$

$$\mathcal{L}_{\text{GC}} = 1 - \frac{\det\left\{\mathbf{Y}^H\mathbf{Y}\right\}}{\prod_{k=1}^{K}\|\mathbf{y}_k\|^2} \underset{\mathcal{H}_0}{\overset{\mathcal{H}_1}{\gtrless}} \zeta_{\text{GC}} \tag{37}$$

$$\mathcal{L}_{\text{RLET}} = \frac{\lambda_1\left(\mathbf{Y}^H\mathbf{Y}\right)}{\sum_{k=1}^{K}\lambda_k\left(\mathbf{Y}^H\mathbf{Y}\right)} \underset{\mathcal{H}_0}{\overset{\mathcal{H}_1}{\gtrless}} \zeta_{\text{RLET}} \tag{38}$$

where $\mathbf{Y} = [\mathcal{D}_1^H\mathbf{y}_1, \mathcal{D}_2^H\mathbf{y}_2, \ldots, \mathcal{D}_K^H\mathbf{y}_K]$, which consists of delay-and-Doppler compensated signals by using (10), and $\lambda_K(\cdot) \le \lambda_{K-1}(\cdot) \le \cdots \le \lambda_2(\cdot) \le \lambda_1(\cdot)$ denote the ordered eigenvalues of a K-dimensional matrix. For easy reference, the GLRT detectors proposed in Sections III-A and III-B are denoted as GLRT_1 and GLRT_2, respectively.

For simplicity, we use a first-order autoregressive (AR) process to simulate the IO waveform, in which case the waveform coefficient can be conveniently controlled by changing the AR coefficient a_1. Let ρ $(0 \le \rho < 1)$ measure the correlation in absolute value of two adjacent samples of the IO waveform. For the considered AR process, we have $\rho = |a_1|$. The signal-to-noise ratio (SNR) for the target echoes is defined as

$$\text{SNR} = 10\log_{10}\frac{1}{K}\sum_{k=1}^{K}\frac{|\alpha_k|^2}{\eta_k} \tag{39}$$

and the DPI-to-noise ratio (DNR) is

$$\text{DNR} = 10\log_{10}\frac{1}{K}\sum_{k=1}^{K}\frac{|\beta_k|^2}{\eta_k}. \tag{40}$$

It is noted that, in the following, the threshold for each method is determined based on a constant false alarm rate (CFAR) of $P_{\text{FA}} = 0.01$.

The detection probability curves versus SNR are plotted in Fig. 2, where the following parameters are used: sample number $M = 20$, receiver number $K = 3$, DNR $= 0$ dB, and two cases of different waveform correlations are considered. In Fig. 2(a), we have $\rho = 0.9$, which corresponds to the case when the IO waveform is highly correlated or, equivalently, narrowband. We see that the GLRT_1 detector performs the best, and the GLRT_2 detector has slightly inferior performance. Both the proposed detectors

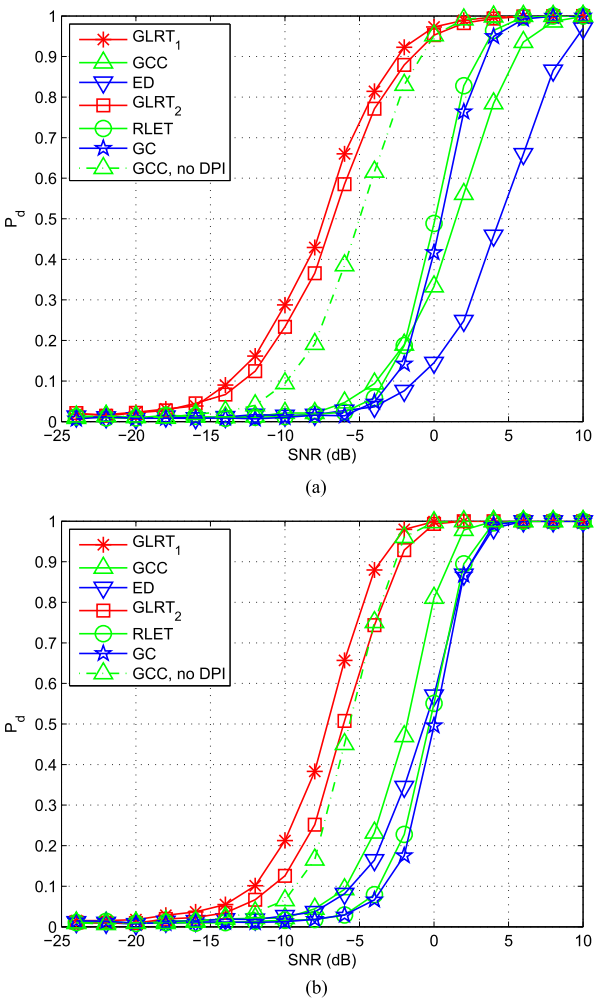

Fig. 2. Performance versus SNR with $M = 20$, $K = 3$, and DNR $= 0$ dB. (a) Highly correlated waveform ($\rho = 0.9$). (b) Lowly correlated waveform ($\rho = 0.001$).

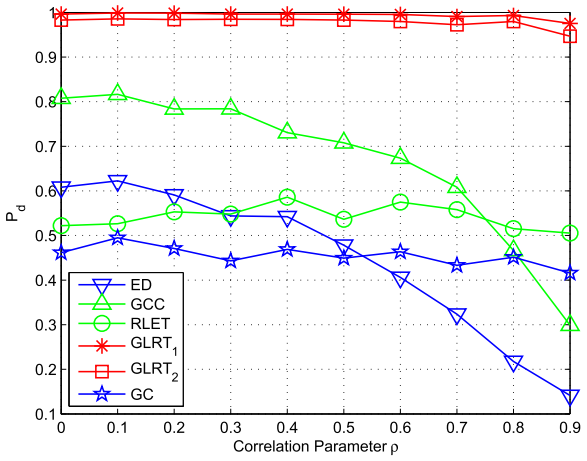

Fig. 3. Performance versus waveform correlation ρ with $M = 20$, $K = 3$, SNR $= 0$ dB, and DNR $= 0$ dB.

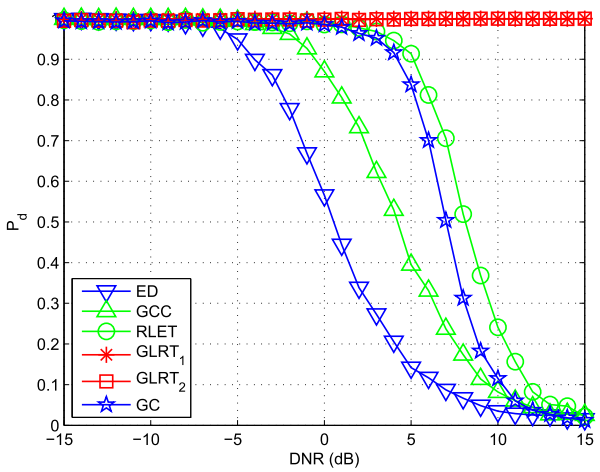

Fig. 4. Performance versus DNR with $M = 20$, $K = 3$, $\rho = 0.9$, and SNR $= 5$ dB.

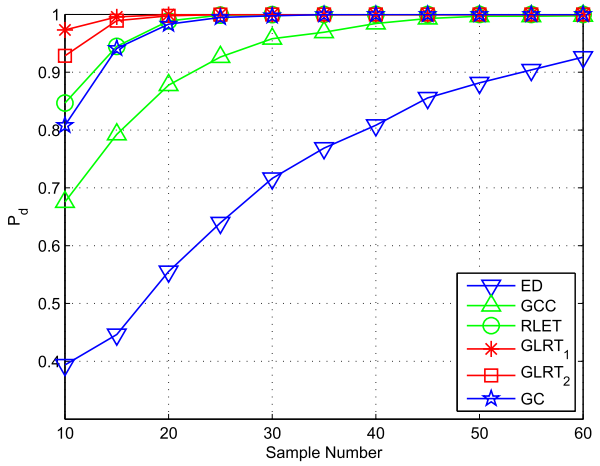

Fig. 5. Performance versus sample number M with $K = 3$, $\rho = 0.9$, SNR $= 5$ dB, and DNR $= 0$ dB.

do however, outperform the other detectors because the formers take into account the residual DPI and, moreover, exploit the waveform correlation for detection. In Fig. 2(b), $\rho = 0.001$ is assumed, which corresponds to a lowly correlated wideband IO signal. In this case, the proposed detectors perform still the best; however, the gain is not as significant as in case 1. The improvement is due to the low waveform correlation, which makes the DPI behave like white noise to the other detectors.

To illustrate the effect of the DPI and, respectively, the effect of the waveform correlation on passive detection, we have included the performance of the GCC detector without DPI.[1] In Fig. 2(a), the proposed detectors perform better than the GCC with no DPI, due to the benefit of using the waveform correlation. In Fig. 2(b), however, the difference between GLRT_2 and GCC is fairly small. This is because, first, there is little waveform correlation that can be utilized by GLRT_2; and second, GLRT_2 has to estimate the noise level, which is assumed to be known by the GCC. Nevertheless, GLRT_1 performs the best among all detectors.

From Fig. 2, we can see that the waveform correlation ρ has an impact on most detectors. To further study this effect, we show the detection performance versus ρ in Fig. 3, where $M = 20$, $K = 3$, SNR $= 0$ dB, and DNR $= 0$ dB. It is seen that the proposed detectors are insensitive as ρ changes from 0 to 0.9. On the other hand, the ED and GCC appear most sensitive to the correlation of the IO waveform.

Fig. 4 shows the performance of the proposed detectors versus DNR with $M = 20$, $K = 3$, $\rho = 0.9$, and SNR $=$ 5 dB. It is observed that the proposed detectors are not affected by the variations in DNR values. On the other hand, the other detectors are significantly affected by the DPI.

Fig. 5 illustrates the performance comparison versus the sample number M used. We can see that increasing M leads to improved detection performance for all detectors. This is because the effective SNR increases with M. Note that (39) is the average SNR per channel and per sample. The improvement for the proposed detectors after $M = 20$ is minor because their detection probability is nearly 1. However, the extra SNR gain leads to significant detection improvement for the other detectors.

In Fig. 6, the performance is presented as a function of the channel number K, where $M = 20$, $\rho = 0.9$, SNR $= 5$ dB, and DNR $= 0$ dB. The proposed detectors still perform the best. It is noted again that as K gets larger, the effective SNR increases. The performances of RLET, GC, and GCC are seen to benefit more from increasing K than the ED. This is because the formers can exploit the coherence among the different channels [14].

Note that the proposed detectors GLRT_1 and GLRT_2 need to know the covariance matrix $\mathbf{C}_x$, equivalently $\mathbf{R}_x$, of the IO signal, which may be unknown and needs to be estimated in practice by using training signals. To illustrate the effect of covariance matrix estimation on the proposed detectors, we consider a simple scenario, where training signals are collected by steering an antenna toward the IO (whose location is usually known) to measure the source signal. The measurements are generally contaminated by

[1]It is noted that in the absence of DPI, the GCC is the best among the four existing detectors (35)–(38) according to [14]. Hence, the results for the other detectors without DPI are not included for clarity.

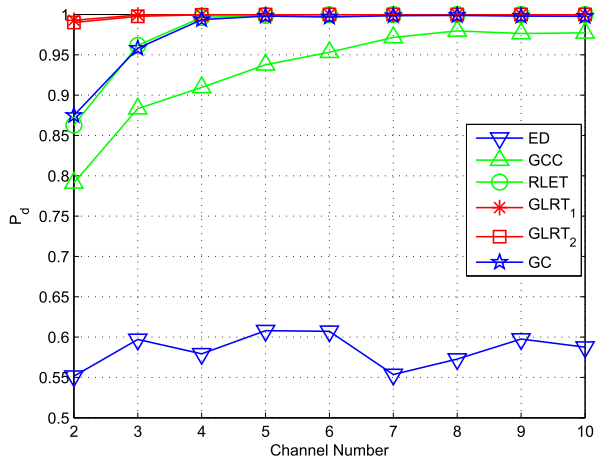

Fig. 6. Performance versus channel number K with $M = 20$, $\rho = 0.9$, SNR $= 5$ dB, and DNR $= 0$ dB.

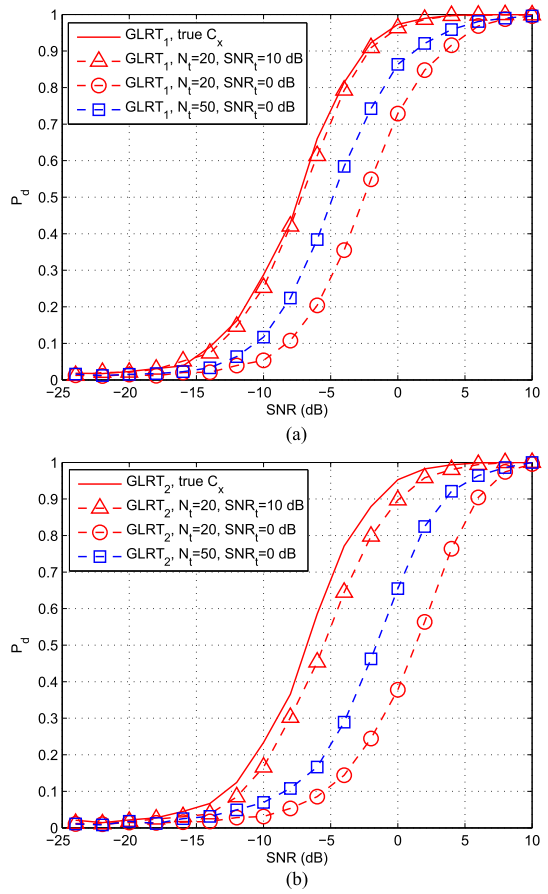

Fig. 7. Performance comparisons using estimated waveform covariance matrix with $M = 20$, $K = 3$, $\rho = 0.9$, and DNR $= 0$ dB. (a) GLRT$_1$. (b) GLRT$_2$.

noise. Let SNR$_t$ denote the SNR in the training signals. Suppose N_t samples of training signals are available. We use the simple unbiased estimator to estimate the autocorrelation function (ACF) of the training signals. The ACF of the IO signal can be obtained by subtracting the noise variance from the former; in the case when the noise variance is unknown (as in GLRT$_2$), the ACF of the training signals is used as the ACF of the IO signal. Following ACF estimation, an estimate of the covariance matrix $\mathbf{R}_x$ can be formed as a Toeplitz matrix by using the ACF along with a tapering window (see [32] for details on how to form a covariance matrix estimate from ACF). The performance of the proposed detectors with estimated $\mathbf{C}_x$ is shown in Fig. 7(a) for GLRT$_1$ and, respectively, in Fig. 7(b) for GLRT$_2$, with several combinations of SNR$_t$ and N_t. It is seen that with sufficiently high SNR$_t$ (e.g., 10 dB), the performance loss of GLRT$_1$ caused by covariance matrix estimation is very small. Although the loss increases with a lower SNR$_t$, it can be remedied by using more training signals in covariance matrix estimation, as seen in the comparison of the case of SNR$_t = 0$ dB and $N_t = 20$ with that of SNR$_t = 0$ dB and $N_t = 50$. Finally, it is observed that GLRT$_2$ experiences more performance loss, due to the fact that a coarser covariance matrix estimate is employed, that is, the noise variance is not subtracted, as noted in the above.

V. CONCLUSION

In this paper, we examined the target detection problem for a multistatic passive radar system in the presence of noise and DPI. The system consists of a noncooperative IO and multiple geographically distributed receivers. We proposed two GLRT detectors based on the EM algorithm. The first detector is developed for the case of known receiver noise level, while the second one is derived under the condition when the noise level is unknown. Numerical results show that the proposed detectors significantly outperform several popular existing solutions, as the formers explicitly account for the DPI and exploit the waveform correlation for detection.

APPENDIX

A. Proof of (18)

With known noise variance, we have the unknown parameters $\boldsymbol{\theta} = \{\boldsymbol{\alpha}, \boldsymbol{\beta}\}$ under $\mathcal{H}_1$, and the likelihood function of the "complete" data $\mathbf{z} = [\mathbf{x}^T, \mathbf{y}^T]^T$ can be written as

$$p(\mathbf{z}|\boldsymbol{\theta}) = p(\mathbf{y}|\mathbf{x}, \boldsymbol{\theta})p(\mathbf{x}|\boldsymbol{\theta}) = \frac{1}{\det\{\pi\mathbf{C}_x\}\det\{\pi\mathbf{C}_n\}} \times \exp\left\{-\mathbf{x}^H\mathbf{C}_x^{-1}\mathbf{x} - \sum_{k=1}^{K}\frac{\|\mathbf{y}_k - \beta_k\mathbf{x} - \alpha_k\mathcal{D}_k\mathbf{x}\|^2}{\eta_k}\right\}. \quad (41)$$

Thus, the LLF is given by

$$\log p(\mathbf{z}|\boldsymbol{\theta}) = s_1(\mathbf{x}) - s_2(\mathbf{x}, \boldsymbol{\theta}) \quad (42)$$

where

$$s_1(\mathbf{x}) = -M(K+1)\ln\pi - \ln\det\{\mathbf{C}_x\} - \mathbf{x}^H\mathbf{C}_x^{-1}\mathbf{x} - \sum_{k=1}^{K}\left(M\ln\eta_k + \frac{\|\mathbf{y}_k\|^2}{\eta_k}\right) \quad (43)$$

$$s_2(\mathbf{x}, \boldsymbol{\theta}) = \sum_{k=1}^{K}\frac{1}{\eta_k}\left[\left(|\beta_k|^2 + |\alpha_k|^2\right)\mathbf{x}^H\mathbf{x} + 2\Re\left\{\alpha_k\beta_k^*\mathbf{x}^H\mathcal{D}_k\mathbf{x} - \beta_k\mathbf{y}_k^H\mathbf{x} - \alpha_k\mathbf{y}_k^H\mathcal{D}_k\mathbf{x}\right\}\right]. \quad (44)$$

The cost function is consequently given by

$$Q\left(\boldsymbol{\theta};\hat{\boldsymbol{\theta}}^{(l)}\right) = E_{\mathbf{x}|\mathbf{y},\hat{\boldsymbol{\theta}}^{(l)}}\left\{s_1(\mathbf{x})\right\} - E_{\mathbf{x}|\mathbf{y},\hat{\boldsymbol{\theta}}^{(l)}}\left\{s_2(\mathbf{x},\boldsymbol{\theta})\right\}. \quad (45)$$

Note that only the second term in (45) involves the parameters to be estimated and that the first term is constant in the M-step for each iteration. Therefore, we have the following result for the M-step,

$$\arg\max_{\boldsymbol{\theta}} Q\left(\boldsymbol{\theta};\hat{\boldsymbol{\theta}}^{(l)}\right) = \arg\min_{\boldsymbol{\theta}} Q_1\left(\boldsymbol{\theta};\hat{\boldsymbol{\theta}}^{(l)}\right) \quad (46)$$

where

$$Q_1\left(\boldsymbol{\theta};\hat{\boldsymbol{\theta}}^{(l)}\right) = E_{\mathbf{x}|\mathbf{y},\hat{\boldsymbol{\theta}}^{(l)}}\left\{s_2(\mathbf{x},\boldsymbol{\theta})\right\}. \quad (47)$$

Next, we find an explicit expression for $Q_1\left(\boldsymbol{\theta};\hat{\boldsymbol{\theta}}^{(l)}\right)$. Since the vectors $\mathbf{x}$ and $\mathbf{y}$ are jointly Gaussian distributed, let

$$\hat{\mathbf{x}}^{(l)} = E_{\mathbf{x}|\mathbf{y},\hat{\boldsymbol{\theta}}^{(l)}}\{\mathbf{x}\} \quad (48)$$

and then the conditional expectation $\hat{\mathbf{x}}^{(l)}$ has a closed-form expression [33, p. 324]. By denoting

$$\begin{aligned}\mathbf{C}_{xy}^{(l)} &= E_{\mathbf{x}|\hat{\boldsymbol{\theta}}^{(l)}}\left\{\mathbf{x}\mathbf{y}^H\right\} \\ &= \left(\hat{\boldsymbol{\beta}}^{(l)}\right)^H \otimes \mathbf{C}_x + \mathbf{C}_x\left(\hat{\boldsymbol{\alpha}}^{(l)} \otimes \mathbf{I}_M\right)^H \mathbf{D}^H \quad (49)\\ \mathbf{C}_{yy}^{(l)} &= E_{\mathbf{x}|\hat{\boldsymbol{\theta}}^{(l)}}\left\{\mathbf{y}\mathbf{y}^H\right\} = \mathbf{C}_y\left(\hat{\boldsymbol{\alpha}}^{(l)}, \hat{\boldsymbol{\beta}}^{(l)}\right) \quad (50)\end{aligned}$$

we have

$$\begin{aligned}\hat{\mathbf{x}}^{(l)} &= E\{\mathbf{x}\} + \mathbf{C}_{xy}^{(l)}\left(\mathbf{C}_{yy}^{(l)}\right)^{-1}\left(\mathbf{y} - E\{\mathbf{y}\}\right) \\ &= \mathbf{C}_{xy}^{(l)}\left(\mathbf{C}_{yy}^{(l)}\right)^{-1}\mathbf{y}. \quad (51)\end{aligned}$$

Consequently,

$$\begin{aligned}\mathbf{C}_{xx|y}^{(l)} &= E_{\mathbf{x}|\mathbf{y},\hat{\boldsymbol{\theta}}^{(l)}}\left\{\mathbf{x}\mathbf{x}^H\right\} \\ &= \hat{\mathbf{x}}^{(l)}\left(\hat{\mathbf{x}}^{(l)}\right)^H + E_{\mathbf{x}|\mathbf{y},\hat{\boldsymbol{\theta}}^{(l)}}\left\{\left(\mathbf{x} - \hat{\mathbf{x}}^{(l)}\right)\left(\mathbf{x} - \hat{\mathbf{x}}^{(l)}\right)^H\right\} \\ &= \hat{\mathbf{x}}^{(l)}\left(\hat{\mathbf{x}}^{(l)}\right)^H + \mathbf{C}_x - \mathbf{C}_{xy}^{(l)}\left(\mathbf{C}_{yy}^{(l)}\right)^{-1}\left(\mathbf{C}_{xy}^{(l)}\right)^H. \quad (52)\end{aligned}$$

Finally, we get

$$\begin{aligned}Q_1\left(\boldsymbol{\theta};\hat{\boldsymbol{\theta}}^{(l)}\right) = \sum_{k=1}^{K}\frac{1}{\eta_k}\Big[&\left(|\beta_k|^2 + |\alpha_k|^2\right)c_1^{(l)} \\ &+ 2\Re\left\{\alpha_k\beta_k^* c_{2,k}^{(l)} - \beta_k c_{3,k}^{(l)} - \alpha_k c_{4,k}^{(l)}\right\}\Big] \quad (53)\end{aligned}$$

where

$$\begin{aligned}c_1^{(l)} &= E_{\mathbf{x}|\mathbf{y},\hat{\boldsymbol{\theta}}^{(l)}}\left\{\mathbf{x}^H\mathbf{x}\right\} = \mathrm{tr}\left\{\mathbf{C}_{xx|y}^{(l)}\right\} \quad (54)\\ c_{2,k}^{(l)} &= E_{\mathbf{x}|\mathbf{y},\hat{\boldsymbol{\theta}}^{(l)}}\left\{\mathbf{x}^H\mathcal{D}_k\mathbf{x}\right\} = \mathrm{tr}\left\{\mathcal{D}_k\mathbf{C}_{xx|y}^{(l)}\right\} \quad (55)\\ c_{3,k}^{(l)} &= E_{\mathbf{x}|\mathbf{y},\hat{\boldsymbol{\theta}}^{(l)}}\left\{\mathbf{y}_k^H\mathbf{x}\right\} = \mathbf{y}_k^H\hat{\mathbf{x}}^{(l)} \quad (56)\\ c_{4,k}^{(l)} &= E_{\mathbf{x}|\mathbf{y},\hat{\boldsymbol{\theta}}^{(l)}}\left\{\mathbf{y}_k^H\mathcal{D}_k\mathbf{x}\right\} = \mathbf{y}_k^H\mathcal{D}_k\hat{\mathbf{x}}^{(l)}. \quad (57)\end{aligned}$$

B. Proof of (28)

When the noise variance is unknown, we have $\boldsymbol{\theta} = \{\boldsymbol{\alpha}, \boldsymbol{\beta}, \boldsymbol{\eta}\}$ under $\mathcal{H}_1$, and the likelihood function of the "complete" data $\mathbf{z} = [\mathbf{x}^T, \mathbf{y}^T]^T$ can be written as

$$\begin{aligned}p(\mathbf{z}|\boldsymbol{\theta}) = p(\mathbf{y}|\mathbf{x},\boldsymbol{\theta})p(\mathbf{x}|\boldsymbol{\theta}) &= \frac{1}{\det\{\pi\mathbf{C}_x\}\det\{\pi\mathbf{C}_n(\boldsymbol{\eta})\}} \\ &\times \exp\left\{-\mathbf{x}^H\mathbf{C}_x^{-1}\mathbf{x} - \sum_{k=1}^{K}\frac{\|\mathbf{y}_k - \beta_k\mathbf{x} - \alpha_k\mathcal{D}_k\mathbf{x}\|^2}{\eta_k}\right\}. \quad (58)\end{aligned}$$

The LLF is given by

$$\log p(\mathbf{z}|\boldsymbol{\theta}) = s_1(\mathbf{x}) - s_2(\mathbf{x},\boldsymbol{\theta}) \quad (59)$$

where

$$s_1(\mathbf{x}) = -M(K+1)\ln\pi - \ln\det\{\mathbf{C}_x\} - \mathbf{x}^H\mathbf{C}_x^{-1}\mathbf{x} \quad (60)$$

$$s_2(\mathbf{x},\boldsymbol{\theta}) = \sum_{k=1}^{K}\left(M\ln\eta_k + \frac{\Delta(\mathbf{x},\alpha_k,\beta_k)}{\eta_k}\right) \quad (61)$$

and

$$\begin{aligned}\Delta(\mathbf{x},\alpha_k,\beta_k) = \|\mathbf{y}_k\|^2 &+ \left(|\beta_k|^2 + |\alpha_k|^2\right)\mathbf{x}^H\mathbf{x} \\ &+ 2\Re\left\{\alpha_k\beta_k^*\mathbf{x}^H\mathcal{D}_k\mathbf{x} - \beta_k\mathbf{y}_k^H\mathbf{x} - \alpha_k\mathbf{y}_k^H\mathcal{D}_k\mathbf{x}\right\}. \quad (62)\end{aligned}$$

As stated in Appendix A, the M-step in this case can be rewritten as

$$\arg\max_{\boldsymbol{\theta}} Q\left(\boldsymbol{\theta};\hat{\boldsymbol{\theta}}^{(l)}\right) = \arg\min_{\boldsymbol{\theta}} Q_2\left(\boldsymbol{\theta};\hat{\boldsymbol{\theta}}^{(l)}\right) \quad (63)$$

where

$$Q_2\left(\boldsymbol{\theta};\hat{\boldsymbol{\theta}}^{(l)}\right) = \sum_{k=1}^{K}\left(M\ln\eta_k + \frac{\hat{\Delta}^{(l)}(\alpha_k,\beta_k)}{\eta_k}\right) \quad (64)$$

and

$$\begin{aligned}\hat{\Delta}^{(l)}(\alpha_k,\beta_k) = \|\mathbf{y}_k\|^2 &+ \left(|\beta_k|^2 + |\alpha_k|^2\right)c_1^{(l)} \\ &+ 2\Re\left\{\alpha_k\beta_k^* c_{2,k}^{(l)} - \beta_k c_{3,k}^{(l)} - \alpha_k c_{4,k}^{(l)}\right\} \quad (65)\end{aligned}$$

with $c_1^{(l)}$, $c_{2,k}^{(l)}$, $c_{3,k}^{(l)}$, and $c_{4,k}^{(l)}$ owning the same expressions as in Appendix A. Nevertheless, for the calculations of $\hat{\mathbf{x}}^{(l)}$ and $\mathbf{C}_{xx|y}^{(l)}$ in (51) and (52), respectively, we use the following result instead of (50)

$$\mathbf{C}_{yy}^{(l)} = \mathbf{C}_y(\hat{\boldsymbol{\alpha}}^{(l)}, \hat{\boldsymbol{\beta}}^{(l)}, \hat{\boldsymbol{\eta}}^{(l)}). \quad (66)$$

REFERENCES

[1] H. D. Griffiths and C. J. Baker
Passive coherent location radar systems. Part 1: Performance prediction
IEE Proc. Radar Sonar Navig., vol. 152, no. 3, pp. 124–132, Jun. 2005.

[2] C. J. Baker, H. D. Griffiths, and I. Papoutsis
Passive coherent location radar systems. Part 2: Waveform properties
IEE Proc. Radar Sonar Navig., vol. 152, no. 3, pp. 160–168, Jun. 2005.

[3] P. E. Howland, D. Maksimiuk, and G. Reitsma
FM radio based bistatic radar
IEE Proc. Radar Sonar Navig., vol. 152, no. 3, pp. 107–115, Jun. 2005.

[4] M. K. Baczyk and M. Malanowski
Reconstruction of the reference signal in DVB-T based passive radar
Int. J. Electron. Telecommun., vol. 57, no. 1, pp. 43–48, Mar. 2011.

[5] Q. He and R. S. Blum
The significant gains from optimally processed multiple signals of opportunity and multiple receive stations in passive radar
IEEE Signal Process. Lett., vol. 21, no. 2, pp. 180–184, Feb. 2014.

[6] X. Zhang, H. Li, J. Liu, and B. Himed
Joint delay and Doppler estimation for passive sensing with direct-path interference
IEEE Trans. Signal Process., vol. 64, no. 3, pp. 630–640, Feb. 2016.

[7] G. Cui, J. Liu, H. Li, and B. Himed
Signal detection with noisy reference for passive sensing
Signal Process., vol. 108, pp. 389–399, Mar. 2015.

[8] D. E. Hack, L. K. Patton, B. Himed, and M. A. Saville
Detection in passive MIMO radar networks
IEEE Trans. Signal Process., vol. 62, no. 11, pp. 2999–3012, Jun. 2014.

[9] D. E. Hack, L. K. Patton, B. Himed, and M. A. Saville
Centralized passive MIMO radar detection without direct-path reference signals
IEEE Trans. Signal Process., vol. 62, no. 11, pp. 3013–3023, Jun. 2014.

[10] K. S. Bialkowski, I. V. L. Clarkson, and S. D. Howard
Generalized canonical correlation for passive multistatic radar detection
In *Proc. IEEE Statist. Signal Process. Workshop*, Jun. 2011, pp. 417–420.

[11] N. Vankayalapati and S. Kay
Asymptotically optimal detection of low probability of intercept signals using distributed sensors
IEEE Trans. Aerosp. Electron. Syst., vol. 48, no. 1, pp. 737–748, Jan. 2012.

[12] L. Wang and B. Yazici
Passive imaging of moving targets using sparse distributed apertures
SIAM J. Imaging Sci., vol. 5, no. 3, pp. 769–808, 2012.

[13] S. Sirianunpiboon, S. D. Howard, and D. Cochran
A Bayesian derivation of generalized coherence detectors
In *Proc. Int. Conf. Acoust. Speech Signal Process.*, Kyoto, Japan, Mar. 2012, pp. 3253–3256.

[14] J. Liu, H. Li, and B. Himed
Two target detection algorithms for passive multistatic radar
IEEE Trans. Signal Process., vol. 62, no. 22, pp. 5930–5939, Nov. 2014.

[15] D. E. Hack, L. K. Patton, and B. Himed
Multichannel detection of an unknown rank-one signal with uncalibrated receivers
In *Proc. IEEE Int. Conf. Acoust. Speech, Signal Process.*, Florence, Italy, May 2014, pp. 2987–2991.

[16] S. Searle, J. Palmer, L. Davis, D. W. O' Hagan, and M. Ummenhofer
Evaluation of the ambiguity function for passive radar with OFDM transmissions
In *Proc. IEEE Radar Conf.*, Cincinnati, OH, USA, May 2014, pp. 1040–1045.

[17] H. Urkowitz
Energy detection of unknown deterministic signals
Proc. IEEE, vol. 55, no. 4, pp. 523–531, Apr. 1967.

[18] P. Wang, J. Fang, N. Han, and H. Li
Multiantenna-assisted spectrum sensing for cognitive radio
IEEE Trans. Veh. Technol., vol. 59, no. 4, pp. 1791–1800, May 2010.

[19] G. C. Carter
Coherence and time delay estimation
Proc. IEEE, vol. 75, no. 2, pp. 236–255, Feb. 1987.

[20] H. Gish and D. Cochran
Generalized coherence
In *Proc. Int. Conf. Acoust. Speech, Signal Process.*, New York, NY, USA, Apr. 1988, pp. 2745–2748.

[21] D. Cochran, H. Gish, and D. Sinno
A geometric approach to multiple-channel signal detection
IEEE Trans. Signal Process., vol. 43, no. 9, pp. 2049–2057, Sep. 1995.

[22] R. Tao, H. Z. Wu, and T. Shan
Direct-path suppression by spatial filtering in digital television terrestrial broadcasting-based passive radar
IET Radar Sonar Navig., vol. 4, no. 6, pp. 791–805, Dec. 2010.

[23] F. Colone *et al.*
Space-time constant modulus algorithm for multipath removal on the reference signal exploited by passive bistatic radar
IET Radar Sonar Navig., vol. 3, no. 3, pp. 253–264, Jun. 2009.

[24] F. Colone, D. W. O'Hagan, P. Lombardo, and C. J. Baker
A multistage processing algorithm for disturbance removal and target detection in passive bistatic radar
IEEE Trans. Aerosp. Electron. Syst., vol. 45, no. 2, pp. 698–722, Apr. 2009.

[25] J. E. Palmer, H. A. Harms, S. J. Searle, and L. M. Davis
DVB-T passive radar signal processing
IEEE Trans. Signal Process., vol. 61, no. 8, pp. 2116–2126, Apr. 2013.

[26] O. Rabaste and D. Poullin
Rejection of Doppler shifted multipaths in airborne passive radar
In *Proc. IEEE Int. Radar Conf.*, Arlington, VA, USA, May 2015, pp. 1660–1665.

[27] D. K. P. Tan, M. Lesturgie, H. Sun, and Y. Lu
Target detection performance analysis for airborne passive bistatic radar
IEEE Int. Geosci. Remote Sens. Symp., Jul. 2010, pp. 3553–3556.

[28] A. P. Dempster, N. M. Laird, and D. B. Rubin
Maximum likelihood from incomplete data via the EM algorithm
J. Roy. Statist. Soc., Series B (Methodological), vol. 39, no. 1, pp. 1–38, 1977.

[29] G. Cui, J. Liu, H. Li, and B. Himed
Target detection for passive radar with noisy reference channel
In *Proc. IEEE Radar Conf.*, Cincinnati, OH, USA, May 2014, pp. 0144–0148.

[30] A. V. Oppenheim, R. W. Schafer, and J. R. Buck
Discrete-Time Signal Processing, 2nd ed. Upper Saddle River, NJ, USA: Prentice-Hall, 1999.

[31] M. A. Richards
Fundamentals of Radar Signal Processing. New York, NY, USA: McGraw-Hill, 2005.

[32] S. M. Kay
Modern Spectral Estimation: Theory and Application. Englewood Cliffs, NJ, USA: Prentice-Hall, 1988.

[33] S. M. Kay
Fundamentals of Statistical Signal Processing: Estimation Theory. Upper Saddle River, NJ, USA: Prentice-Hall, 1993.

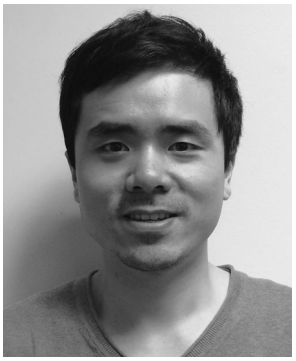

Xin Zhang received the B.Eng. degree (with honors) from the University of Science and Technology Beijing, Beijing, China, in 2008, and the M.Eng. degree from Beijing University of Posts and Telecommunications (BUPT), Beijing, China, in 2011, both in electrical engineering. He is currently working toward the Ph.D. degree in electrical engineering at Stevens Institute of Technology, Hoboken, NJ, USA.

He has been a Research and Teaching Assistant in the Department of Electrical and Computer Engineering, Stevens Institute of Technology, Hoboken, NJ, USA, since 2013. His research interests include statistical signal processing, optimization algorithms, passive sensing, and multichannel signal processing.

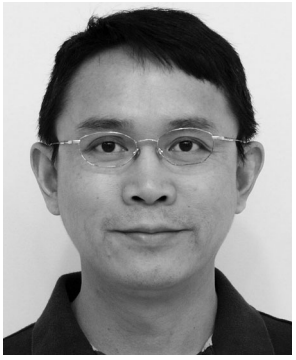

Hongbin Li (M'99–SM'08) received the B.S. and M.S. degrees from the University of Electronic Science and Technology of China, Chengdu, China, in 1991 and 1994, respectively, and the Ph.D. degree from the University of Florida, Gainesville, FL, USA, in 1999, all in electrical engineering.

From July 1996 to May 1999, he was a Research Assistant in the Department of Electrical and Computer Engineering, University of Florida. Since July 1999, he has been with the Department of Electrical and Computer Engineering, Stevens Institute of Technology, Hoboken, NJ, USA, where he became a Professor in 2010. He was a Summer Visiting Faculty Member at the Air Force Research Laboratory in the summers of 2003, 2004, and 2009. His general research interests include statistical signal processing, wireless communications, and radars.

Dr. Li received the IEEE Jack Neubauer Memorial Award in 2013 from the IEEE Vehicular Technology Soceity, the Outstanding Paper Award from the IEEE AFICON Conference in 2011, the Harvey N. Davis Teaching Award in 2003 and the Jess H. Davis Memorial Award for excellence in research in 2001 from Stevens Institute of Technology, and the Sigma Xi Graduate Research Award from the University of Florida in 1999. He has been a member of the IEEE SPS Signal Processing Theory and Methods Technical Committee and the IEEE SPS Sensor Array and Multichannel TC, an Associate Editor of *Signal Processing* (Elsevier), the IEEE TRANSACTIONS ON SIGNAL PROCESSING, the IEEE SIGNAL PROCESSING LETTERS, and the IEEE TRANSACTIONS ON WIRELESS COMMUNICATIONS, as well as a Guest Editor of the IEEE JOURNAL OF SELECTED TOPICS IN SIGNAL PROCESSING and the EURASIP *Journal on Applied Signal Processing*. He has been involved in various conference organization activities, including serving as a General Co-Chair for the 7th IEEE Sensor Array and Multichannel Signal Processing Workshop, Hoboken, NJ, USA, June 17–20, 2012. He is a member of Tau Beta Pi and Phi Kappa Phi.

Braham Himed (F'07) received the Engineer Degree in electrical engineering from Ecole Nationale Polytechnique of Algiers, El-Harrach, Algeria, in 1984, and the M.S. and Ph.D. degrees both in electrical engineering, from Syracuse University, Syracuse, NY, USA, in 1987 and 1990, respectively.

He is a Technical Advisor with the Air Force Research Laboratory, Sensors Directorate, RF Technology Branch, Dayton, OH, USA, where he is involved with several aspects of radar developments. His research interests include detection, estimation, multichannel adaptive signal processing, time series analyses, array processing, adaptive processing, waveform diversity, distributed active/passive radar, and over-the-horizon radar.

Dr. Himed received the 2001 IEEE region I award for his work on bistatic radar systems, algorithm development, and phenomenology and the 2012 IEEE Warren White award for excellence in radar engineering. He is the Chair of the AES Radar Systems Panel. He is also a Fellow of AFRL (class of 2013).